Available online at website: https://journal.bcrec.id/index.php/bcrec

Bulletin of Chemical Reaction Engineering & Catalysis, 20 (2) 2025, 359-370

Original Research Article

Tunable Optical and Photoluminescence Properties of Metal X (Ni, Co, Mn, Ag)-Doped ZnSe Quantum Dots: Structural, Spectroscopic, and Colorimetric Analysis

Thi Diem Bui[1*], Quang Liem Nguyen[2], Nguyen Van Cuong[1], Trong Tang Nguyen[1], Phuc Huu Dang[3*]

[1]Faculty of Chemical Engineering, Industrial University of Ho Chi Minh City, Ho Chi Minh City 700000, Vietnam
[2]Institute of Materials Science, Vietnam Academy of Science and Technology, 18 Hoang Quoc Viet, Hanoi 10000, Vietnam
[3]Faculty of Fundamental Science, Industrial University of Ho Chi Minh City, Ho Chi Minh City, 700000, Vietnam

Received: 19th March 2025; Revised: 23th April 2025; Accepted: 24th April 2025
Available online: 26th April 2025; Published regularly: August 2025

Abstract

This study explores the impact of Ni, Co, Mn, and Ag doping on the optical and photoluminescence properties of ZnSe quantum dots (QDs). Structural analysis confirms successful dopant incorporation, with XRD revealing lattice strain-induced shifts. Optical studies show that Ni^{2+} and Co^{2+} induce blue shifts, while Mn^{2+} and Ag^{+} create redshifted emissions. Photoluminescence analysis demonstrates that Mn^{2+} doping enhances quantum efficiency to 49.52% via the $^4T_1 \rightarrow {}^6A_1$ transition. Ag^{+}-doped ZnSe exhibits blue-shifted emissions but suffers from defect-related non-radiative losses. CIE color coordinates validate tunable emissions, confirming potential applications in LEDs, displays, and bioimaging. These findings provide insights into dopant-induced band structure modifications, advancing the design of high-performance luminescent materials for optoelectronics.

Keywords: ZnSe Quantum Dots; Metal-Doped Semiconductors; Transition Metal Doping; Fluorescence Quantum Yield; CIE

How to Cite: Bui, T. D., Nguyen, Q. L., Nguyen, V. C., Nguyen, T. T., Dang, H. P. (2025). Tunable Optical and Photoluminescence Properties of Metal X (Ni, Co, Mn, Ag)-Doped ZnSe Quantum Dots: Structural, Spectroscopic, and Colorimetric Analysis. *Bulletin of Chemical Reaction Engineering & Catalysis*, 20 (2), 359-370. (doi: 10.9767/bcrec.20372)

Permalink/DOI: https://doi.org/10.9767/bcrec.20372

1. Introduction

Nanomaterials, particularly semiconductor quantum dots (QDs), have gained significant attention because of their unique optical, electronic, and structural properties compared with their bulk counterparts [1-4]. Scientists have concentrated their study on the fabrication process and physical and chemical properties of group II-VI semiconductor nanoparticles, which are straight bandgap semiconductors with high quantum efficiency and are suited for lighting and energy conversion applications [2,4]. Among various QD materials, ZnSe has emerged as a promising candidate due to its wide bandgap (~2.7 eV), high thermal and chemical stability, and environmentally benign nature compared to toxic cadmium-based QDs [6-9]. However, their practical applications in optoelectronics, bio-imaging, and sensing [10-12] are often limited by low quantum efficiency and a narrow emission spectrum. To overcome these challenges, doping with transition and noble metals has been

* Corresponding Author.
Email: buithidiem@iuh.edu.vn (T. D. Bui)
danghuuphuc@iuh.edu.vn (H. P. Dang)

explored as an effective strategy for modifying the electronic structure, enhancing radiative recombination, and improving the emission characteristics.

The incorporation of metal dopants into ZnSe QDs introduces localized electronic states within the bandgap, which significantly influences charge carrier dynamics and optical transitions [13,14]. Transition metal ions (Ni^{2+}, Co^{2+}, Mn^{2+}) and noble metal ions (Ag^{+}) have been extensively investigated owing to their electronic configurations and interactions with the host lattice. These dopants are selected for their ability to modulate emission properties by altering band structure and defect states: Ni^{2+} and Co^{2+}: With smaller ionic radii than Zn^{2+} (0.69 Å for Ni^{2+}, 0.72 Å for Co^{2+}, 0.74 Å for Zn^{2+}), they cause lattice contraction. This leads to increased bandgap energy, blue shifts in the photoluminescence spectra, and enhanced charge carrier recombination via new intermediate states [14,15]. Mn^{2+}: Known for orange-yellow emission via the $^4T_1 \rightarrow {}^6A_1$ transition, Mn^{2+} has a larger ionic radius (0.8 Å) than Zn^{2+}. It enhances fluorescence quantum efficiency by acting as an efficient radiative recombination center suitable for display and lighting applications [16]. Ag^{+}: With a 1.14 Å ionic radius, Ag^{+} incorporation causes lattice expansion and introduces shallow donor states [17]. Ag-doped ZnSe QDs show blue-shifted emissions but increased non-radiative recombination owing to defect-related trap states. The optical and photoluminescence properties of ZnSe:X QDs vary depending on the dopant type and concentration. ZnSe: Ni exhibits blue fluorescence at 444 nm (77.2% high photoluminescence quantum yield), ZnSe: Co shows yellow-green emission at 565 nm (28.79% quantum efficiency). Mn doping produces an orange-yellow emission at 591 nm, with the highest quantum efficiency of 49.52%. Ag-doped ZnSe emitted blue light at 442 nm with a 2-quantum efficiency of 22.48%. The ability to modulate the emission color through selective doping highlights the potential of ZnSe: X QDs for optoelectronic devices, LEDs, display technologies, and bioimaging systems.

This study comprehensively analyzes the structural, optical, and photoluminescence properties of Ni, Co, Mn, and Ag-doped ZnSe QDs. By examining the effects of these dopants on band structure modifications, quantum efficiency, and emission tunability, this study establishes a fundamental understanding of dopant-induced electronic effects. The findings contribute to the rational design of high-performance luminescent materials for next-generation optoelectronic applications.

2. Materials and Method

2.1 Materials

High-purity chemical reagents are used for the synthesis of ZnSe QDs and their doped counterparts. Zinc acetate dihydrate ($Zn(CH_3COO)_2 \cdot 2H_2O$, Merck) was used as the Zn precursor, and sodium selenosulfate (Na_2SeSO_3, Merck) served as the Se source. The doping metals nickel chloride ($NiCl_2$, Merck), cobalt chloride ($CoCl_2$, Merck), manganese chloride ($MnCl_2$, Merck), and silver nitrate ($AgNO_3$, Merck) were introduced in controlled amounts to achieve the desired doping concentration. 3-Mercaptopropionic acid (MPA, Sigma-Aldrich) was employed as a stabilizing agent to enhance the solubility and stability of QDs in aqueous media. Ammonium hydroxide (NH_4OH, Merck) was used to adjust the pH of the reaction mixture to ensure the optimal conditions for QD formation. Deionized (DI) water was used throughout the synthesis process to maintain the purity of the samples.

2.2 Synthesis ZnSe:X MPA (X: Ni, Co, Mn, Ag) or ZnSe MPA

The synthesis of ZnSe:X MPA QDs was carried out in an aqueous medium using a chemical precipitation method (Scheme 1). In a 250 mL round-bottom flask, 10 mL of a 0.1 M $Zn(CH_3COO)_2$ solution was mixed with 90 mL of deionized water under continuous stirring. Subsequently, 40 mL of 0.1 M MPA was added as a stabilizing agent, ensuring efficient capping of the quantum dots to improve their dispersion and prevent aggregation. The doping metal ions (Ni^{2+}, Co^{2+}, Mn^{2+}, or Ag^{+}) were introduced by adding an appropriate volume of a 0.01 M solution of $NiCl_2$, $CoCl_2$, $MnCl_2$, or $AgNO_3$ to achieve a final dopant concentration of 5 mol% relative to Zn^{2+}. The reaction mixture was stirred for 15 min to allow the uniform distribution of the metal ions. To adjust the pH of the solution to 7, a controlled

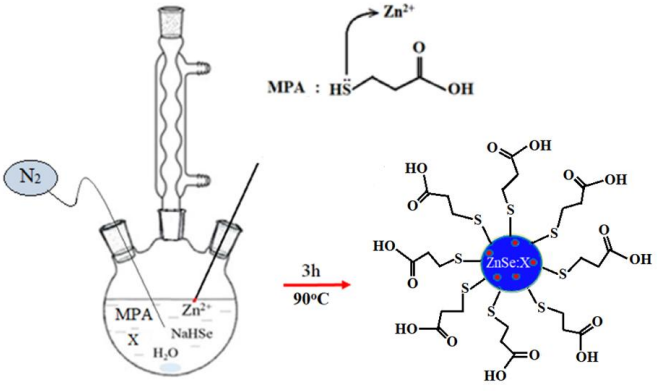

Scheme 1. Synthesis of the ZnSe:X (X: Ni, Co, Mn, Ag) MPA.

amount of 2 M NH_4OH was added dropwise while monitoring the pH. The temperature of the reaction system gradually increased to 90 °C under continuous stirring. Once the desired temperature was reached, an equimolar amount of the NaHSe solution was introduced as the Se source, and the reaction was allowed to proceed for 3 h to ensure the complete formation of ZnSe:X QDs. Upon completion, the reaction mixture was cooled to room temperature, purified by repeated centrifugation, and washed with deionized water to remove unreacted precursors and excess stabilizers. The obtained ZnSe:X MPA QDs were dispersed in deionized water for further characterization.

3. Results and discussion

The XRD pattern of the ZnSe MPA QDs synthesized at 90 °C and pH of 7 shows a cubic crystal structure (zinc blende) due to diffraction peaks at 27.37°, 45.47°, and 54.17 °corresponding to the (111), (220), and (311) planes, respectively, which are consistent with the JCPDS 012-6803 standard card. Metal X (Ni, Co, Mn, and Ag) doping at 90 °C, pH 7, and 5% X^{n+}/Zn^{2+} concentration showed no effect on the crystal phase composition. This outcome is in line with the findings of other research that has been published in studies [18–22]. The impact of doping on the ZnSe lattice is evident in the peak shifts observed in the XRD patterns. Doping with Ni and Co (Ni^{2+} (0.69 Å) and Co^{2+} (0.72 Å)), which have smaller ionic radii than Zn^{2+} (0.74 Å), resulted in a slight shift of the diffraction peaks toward higher 2θ angles, indicating lattice contraction [23–25]. In contrast, Mn and Ag doping led to peak shifts toward lower 2θ angles due to their larger ionic radii (Mn^{2+} (0.8 Å) and Ag^{+} (1.14 Å), suggesting lattice expansion (Figure 1). The outcome is in line with the previous reports [26,27].

The values of the lattice constant a, average crystallite size, particle size, and dislocation density were calculated from equations 1 to 3 and are shown in Table 1. The lattice constants a of QDs with a cubic structure were determined using the following formulas [28,29]:

$$a = b = c = \frac{\lambda}{2\sin\theta}\sqrt{h^2 + k^2 + l^2} \quad (1)$$

where, (hkl) is the Miller index of the crystal plane, θ is the Bragg diffraction angle, and λ = 1.5406 Å is the wavelength of the X-ray.

The broadening of the diffraction peaks was used to compute the average crystallite size of the particles using the Debye-Scherrer equation [30,31]:

$$D = \frac{4}{3}\frac{k\lambda}{\beta\cos\theta} \quad (2)$$

where, λ is the X-ray wavelength, θ is the Bragg angle in radians, β is the breadth at the half-maximum of the peak in radians, D is the particle size, and k is a constant with a value of 0.9.

$$\delta = \frac{n}{D^2} \quad (3)$$

The expression, where n is a constant, was used to calculate the dislocation density δ, which is defined as the total length of dislocation lines per

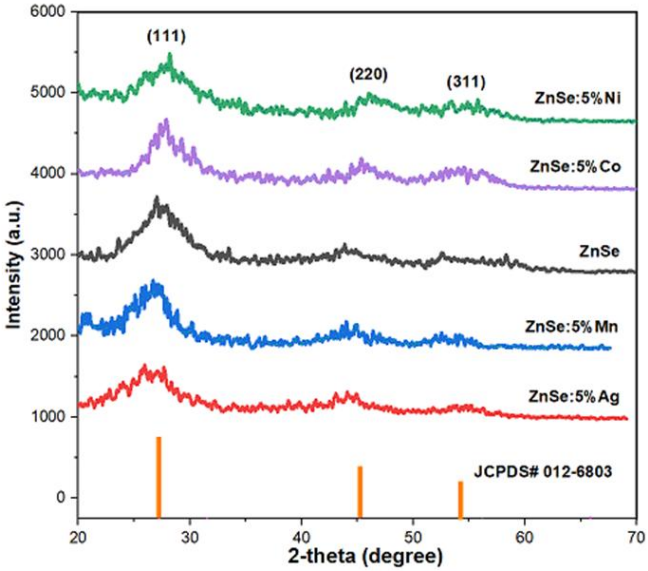

Figure 1. a) The XRD results and HRTEM image of ZnSe:X (X: Ni, Co, Mn, Ag) MPA QDs synthesized at pH of 7 and 90 °C with Xn^{+}/Zn^{2+} ratio of 5%

Table 1. Lattice constant (a), the average crystallite size (D), and dislocation density (δ) of nanoparticle crystallites.

Samples	2θ (°)	(hkl)	$a = b = c$ (Å)	D (nm)	δ (nm^{-2})
ZnSe:5%Ni MPA	27.86	111	5.542	5.792	0.02980
ZnSe:5%Co MPA	27.83	111	5.548	6.413	0.02431
ZnSe MPA	27.64	111	5.585	7.053	0.02010
ZnSe:5%Mn MPA	27.47	111	5.619	7.916	0.01596
ZnSe:5%Ag MPA	27.08	111	5.699	9.147	0.01195

unit crystal volume or, equivalently, as the number of dislocations that intersect a unit area of a random section. The value of δ is typically approximately one [32,33].

The parameters that were determined are listed in Table 1. Doping Co and Ni into the ZnSe lattice changed the lattice properties and dislocation density of ZnSe. Furthermore, The average crystallite size decreased from 7.053 nm (undoped) to 5.792 nm (Ni-doped) and 6.413 nm (Co-doped), while the dislocation density increased from 0.02010 nm^{-2} to 0.02980 nm^{-2} (Ni-doped) and 0.02431 nm^{-2} (Co-doped), whereas Mn and Ag incorporation led to an increase in size. This trend aligns with the observed changes in the lattice constants and dislocation densities, further supporting the successful substitution of Zn^{2+} with dopant ions. The absence of additional peaks corresponding to secondary phases confirms the homogeneous incorporation of metal ions within the ZnSe lattice, rather than the formation of separate metal clusters or oxide phases. These structural modifications resulting from metal doping have direct implications for the optical properties of ZnSe QDs, influencing their emission characteristics and expanding their potential application in optoelectronic devices.

Table 1 demonstrates that doping ZnSe QDs with Co and Ni reduced the lattice constant and average crystallite size (D) and increased the dislocation density. Co^{2+} (0.72 Å) and Ni^{2+} (0.69 Å) have smaller ionic radii compared to Zn^{2+} (0.74 Å). This result also shows that some Zn^{2+} ions are replaced by Co^{2+} and Ni^{2+} ions. When the ZnSe QDs were doped with Mn^{2+} and Ag^{+}, the lattice constant (a) and average crystallite size (D) increased, while the dislocation density decreased [34,35]. This suggests that Zn^{2+} ions were replaced by Mn^{2+} and Ag^{+} ions, as the radius of Mn (0.8 Å) and Ag (1.14 Å) was larger than the radius of Zn (0.74 Å).

3.1 Compositional Studies

Energy-dispersive X-ray spectroscopy (EDX) was utilized to confirm the elemental composition and evaluate the successful incorporation of Ni, Co, Mn, and Ag dopants into the ZnSe QDs (Figure 2). The elemental mapping confirmed the presence of Zn and Se, along with distinct signals corresponding to the respective dopant ions. Notably, carbon and oxygen were also detected, originating from 3-mercaptopropionic acid (MPA) molecules capping the QDs' surfaces. The Zn-to-Se atomic ratio was observed to be greater than unity, indicating a Zn-rich surface, which is typical due to the higher chemical reactivity of Zn^{2+} compared to Se^{2-} during colloidal synthesis. The compositional analysis also revealed that the actual dopant-to-Zn^{2+} ratio X^{n+}/Zn^{2+} was consistently lower than the theoretical value. This discrepancy suggests that a portion of the dopant ions were not incorporated into the ZnSe lattice and may have been removed during purification, a phenomenon commonly observed in colloidal nanocrystal doping. Dopant distribution played a crucial role in determining the structural and optical characteristics of the QDs. Ni and Co doping yielded a more uniform elemental distribution, which promoted efficient charge carrier recombination and enhanced photoluminescence. In contrast, Mn and Ag doping induced localized lattice distortions and potential defect states, which influenced the emission spectra and quantum yield negatively in the case of Ag. These findings are consistent with previous studies reporting that homogeneous doping improves optical performance, while inhomogeneous incorporation or oversized dopant ions can introduce defect-related non-radiative pathways [36–38].

Fourier transform infrared (FT-IR) spectra were obtained to determine the functional groups of the QDs. The FT-IR spectra of MPA and ZnSe:5%Ni MPA QDs, ZnSe:5%Co MPA QDs, ZnSe:5%Mn MPA QDs, and ZnSe:5%Ag MPA QDs (Figure 3) synthesized at pH 7 with a reaction time of 3 h revealed that the vibration peaks corresponding to the wave numbers 3400 cm^{-1} and 3150 cm^{-1} are characteristic vibrations of O-H bonds and water adsorbed on the material surface [39]. The peak at 2890 cm^{-1} was due to the vibration of the -CH_2 group bond. The peaks at 1600 cm^{-1} and 1730 cm^{-1} represent the vibrations of the carboxyl group bond (-C=O). The signal at 1600 cm^{-1}, which corresponds to the carboxyl group (-C=O) of MPA in a neutral medium, was shifted to 1730 cm^{-1} in an alkaline medium. The

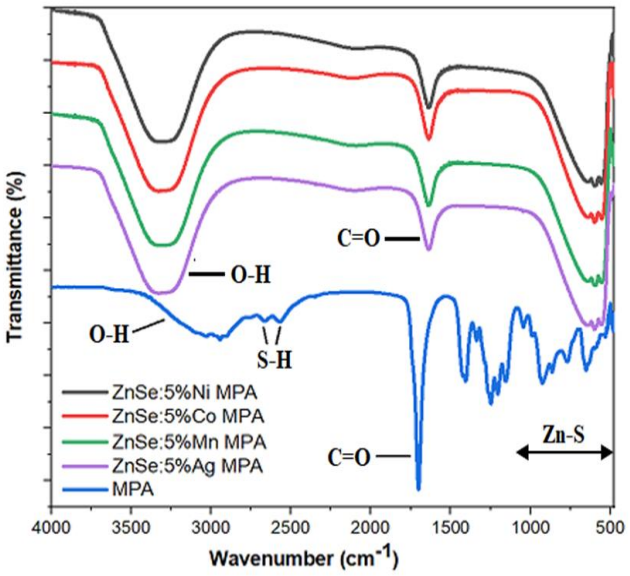

Figure 3. FT-IR spectrum of ZnSe MPA QDs, ZnSe:X MPA (X:Ni, Co, Mn, Ag) QDs synthesized at 90 °C, pH of 7, and at reaction times of 3 h.

peaks at 2520 cm^{-1} and 2650 cm^{-1} are characteristic vibrations of the -S-H bond [24,31,32]. The peaks at 1110 cm^{-1} - 475 cm^{-1} are characteristic vibrations of the Zn-S bond [33, 34]. As a result, the functional group -S-H of MPA is no longer present, while the vibration peaks–OH and–C=O of the -COOH group of MPA remain, demonstrating that MPA is linked with QDs particles and that -SH has formed bonds on the surface of ZnSe crystals. By improving their

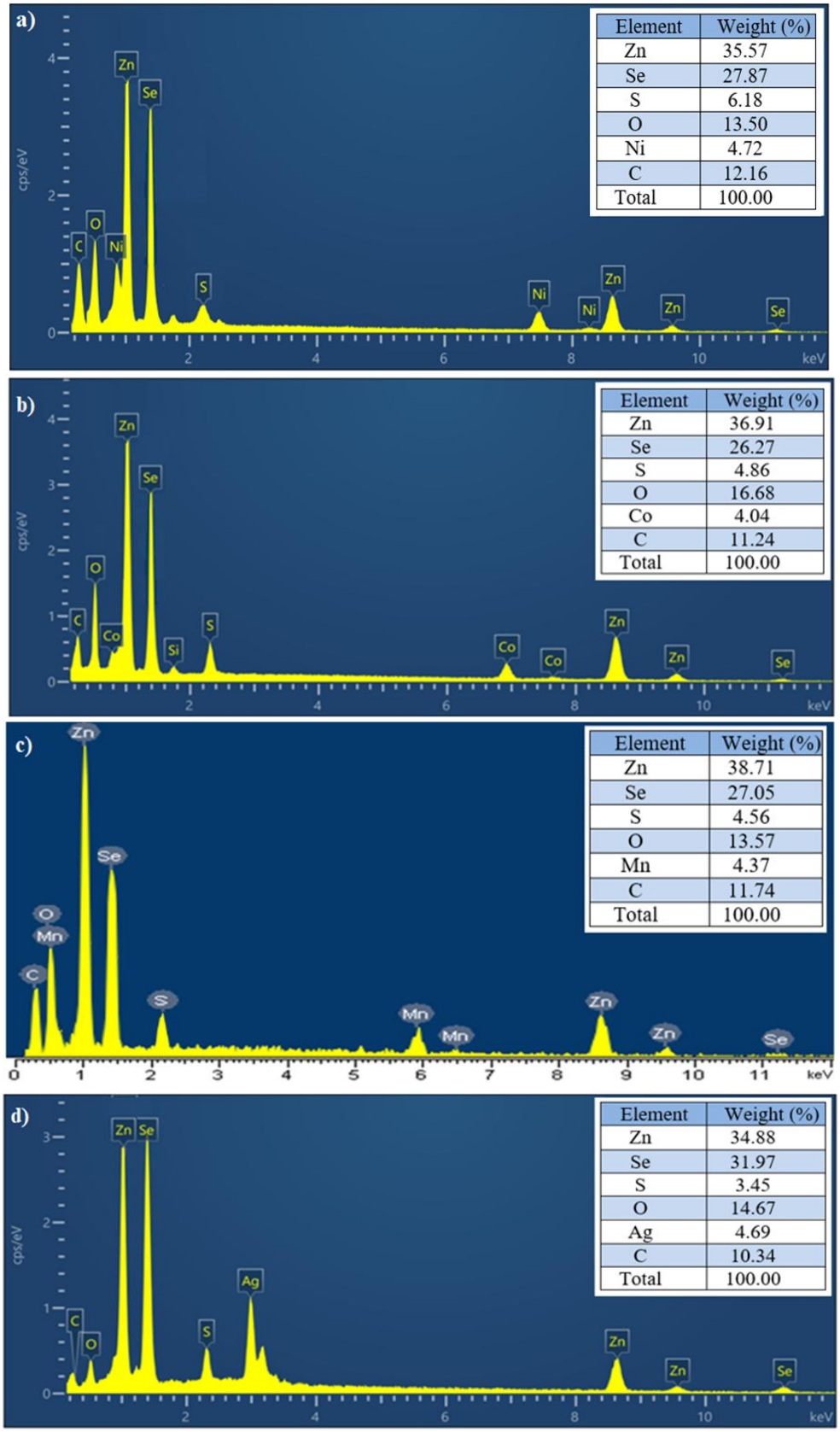

Figure 2. EDX spectra of (a) ZnSe:5%Ni MPA QDs, (b) ZnSe:5%Co MPA QDs, (c) ZnSe:5%Mn MPA QDs, (d) ZnSe:5%Ag MPA QDs synthesized at pH of 7 and 90 °C.

dispersibility in water, these linkages enable the use of ZnSe particles in a wider range of applications, including biology [44].

3.2 Optical Properties

UV-Vis absorption spectroscopy is a powerful method for studying the effects of doping on the optical properties of ZnSe QD. Figure 4 shows the absorption spectra of the ZnSe QDs. The optical properties of the ZnSe and metal-doped ZnSe QDs were investigated using UV-Vis absorption spectroscopy. The absorption edge of the ZnSe QDs exhibited shifts depending on the type of dopant, which was attributed to variations in quantum confinement and electronic structure. Ni and Co doping resulted in a blue shift of the absorption edge, suggesting enhanced quantum confinement owing to lattice contraction. The reduced lattice parameter in these samples increased the bandgap energy, leading to a shift toward shorter wavelengths [14,15,45]. Conversely, Mn and Ag doping induced a redshift in the absorption edge, which can be attributed to lattice expansion and defect-state formation. The larger ionic radii of Mn and Ag cause localized lattice distortions, introducing mid-gap energy states that effectively decrease the bandgap energy and shift the absorption edge toward longer wavelengths [17,46]. These modifications in the absorption properties directly correlate with changes in the photoluminescence characteristics of the doped ZnSe QDs, demonstrating the tunability of their optical response through selective doping strategies.

3.3 Photoluminescence Properties

The fluorescence of ZnSe:X MPA nanocrystals at molar ratios of 5% X^{n+}/Zn^{2+} with varying luminescence intensities is shown in Figure 5. The

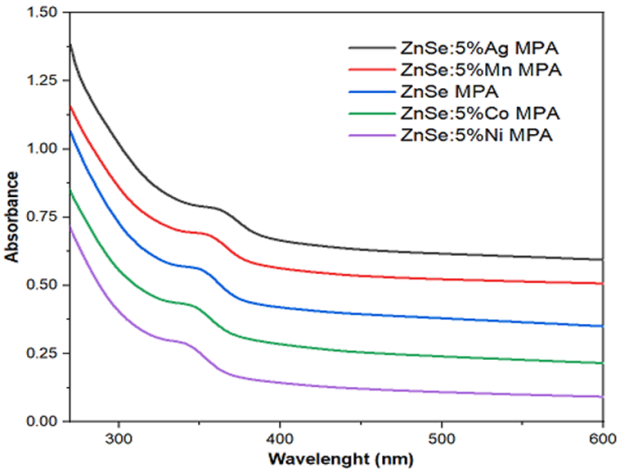

Figure 4. The UV-Vis spectra of ZnSe:X MPA (X:Ni, Co, Mn, Ag) QDs synthesized at 90 °C and pH of 7.

luminous characteristics of QDs are mostly determined by the luminescence intensity at the X^{n+} luminescent center. The photoluminescence (PL) spectra of the ZnSe QDs and ZnSe doped with Ni, Co, Mn, and Ag were obtained at an excitation wavelength of 325 nm to investigate the optical properties of the materials (Figure 5a, b, c a d, e, f)). The PL spectra revealed that doping significantly influenced both the emission wavelength and intensity. The ZnSe:Ni QDs exhibited a strong blue emission at 473 nm, corresponding to the well-known $^3A_2 \rightarrow {}^3T_1$ transition of Ni^{2+} ions. The ZnSe:Co QDs emitted at 565 nm, showing yellow-green fluorescence resulting from electronic transitions within the Co^{2+} dopant levels, corresponding to the well-known $^4T_1 \rightarrow {}^4A_1$ transition of Co^{2+} ions. Mn-doped ZnSe exhibited an intense orange-yellow emission centered at 591 nm, corresponding to the well-known $^4T_1 \rightarrow {}^6A_1$ transition of Mn^{2+} ions. Ag doping led to a blue emission peak at 442 nm, corresponding to the well-known $^1S_o \rightarrow {}^3D_1$ transition of Ag^+ ions ,which is associated with donor-acceptor recombination and defect states within the ZnSe matrix. The CIE color (Fig 5g) coordinates of the ZnSe:X QDs were determined to analyze the effect of metal doping on emission color. The ZnSe:Ni QDs exhibited blue fluorescence with CIE coordinates near (0.15, 0.09), indicating a shift toward the blue region. ZnSe:Co QDs emitting yellow-green light showed CIE coordinates around (0.37, 0.49), which is characteristic of greenish-yellow luminescence. Mn doping resulted in an orange-yellow emission with coordinates of approximately (0.52, 0.42), aligning with warm-colored light applications. Ag^+-doped ZnSe exhibited blue emission with CIE coordinates of approximately (0.20, 0.15), indicating a shift toward a slightly greener blue compared to undoped ZnSe. The CIE diagram confirms that metal doping enables fine-tuning of the emission wavelengths, allowing for precise control over the color output. These tunable optical properties make ZnSe:X QDs highly suitable for applications in display technologies, white-light LEDs, and bioimaging, where precise color rendering is critical.

Fluorescence quantum efficiency (QE) is a precise assessment of the ratio of emitted photons to absorbed photons in a material. The quantum yields (QYs) of the QDs were calculated by comparing them with the quantum-efficient luminescence of organic pigments such as rhodamine, rhodamine 6G, fluorescein 27, and coumarin 153 [35,36,37]. The relative quantum efficiency was estimated using the following formula [38,39]:

$$\emptyset_{f,x} = \emptyset_{f,st}. \frac{Fx}{Fst} \quad (4)$$

Fx and Fst are the fluorescence emission integral areas of the QDs and the Rhodamine B reference, respectively. We utilized Rhodamine B as a standard to calculate the fluorescence quantum efficiency of the manufactured samples, which was 65 % [52,53]. The fluorescence

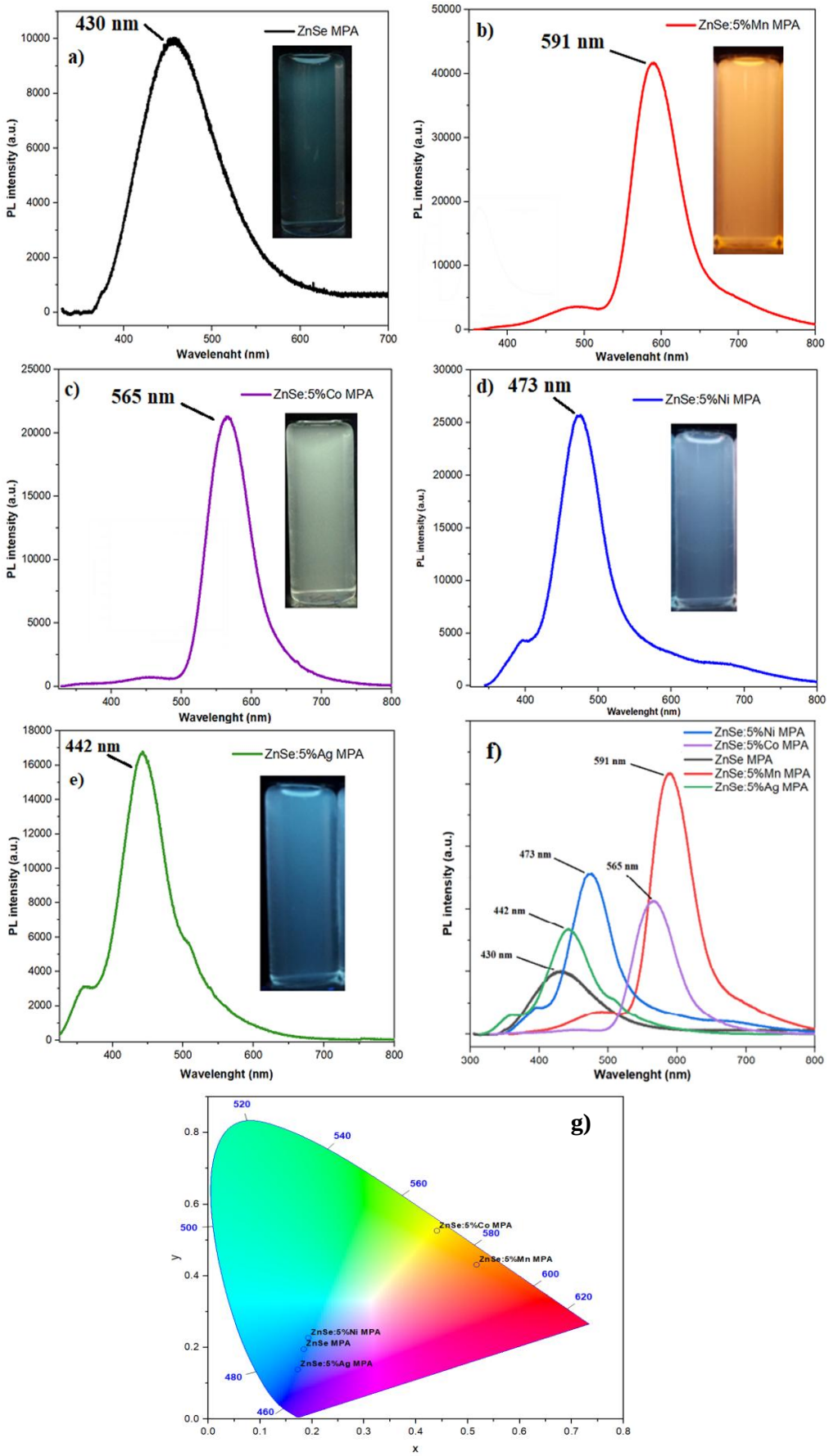

Figure 5. a, b, c, d, e, f) PL spectrum, UV 365 nm image inset and g) CIE color coordinate of ZnSe:X MPA (X: Ni, Co, Mn, Ag) QDs synthesized at 90 °C, pH of 7.

quantum efficiencies of the QDS particles are listed in Table 2.

Fluorescence quantum efficiency (QE) was calculated by comparing the integrated PL intensities of the doped ZnSe QDs with a known standard reference. These results indicate a substantial improvement in the QE upon metal doping. The Mn-doped ZnSe QDs exhibited the highest QE (49.52%), followed by Ni (34.56%), Co (28.79%), and Ag (22.48%). The enhanced QE of the Mn- and Ni-doped samples can be attributed to the introduction of efficient radiative recombination centers, which minimize non-radiative losses. In contrast, Co and Ag doping introduced additional electronic states that facilitated nonradiative recombination, leading to slightly lower quantum yields.

3.4 Proposed Mechanisms

This phenomenon can be attributed to the substitution of X^{n+} ions with Zn^{2+} ions in the ZnSe host material (Scheme 2). The mechanism by which dopant ions (X^{n+} = Ni^{2+}, Co^{2+}, Mn^{2+}, and Ag^{+}) replace Zn^{2+} in the ZnSe lattice plays a crucial role in determining the photoluminescence properties and fluorescence quantum efficiency (QE) of the resulting QDs (Scheme 3). When Zn^{2+} ions are substituted with smaller or larger dopant ions, lattice distortions occur, which influence the electronic band structure and defect states. Ni^{2+} and Co^{2+} substitution: Owing to their smaller ionic radii, Ni^{2+} and Co^{2+} ions induce lattice contraction, which increases the bandgap energy, resulting in a blue shift in photoluminescence. The presence of these transition metal ions introduces new energy levels within the bandgap, facilitating enhanced carrier recombination and improving QE. However, Co^{2+}, known for its strong spin-orbit coupling, creates localized electronic states that slightly reduce the QE compared to Ni^{2+}-doped ZnSe. Mn^{2+} Substitution: The incorporation of Mn^{2+} ions, with a slightly larger ionic radius than that of Zn^{2+}, causes moderate lattice expansion. This expansion results in the formation of Mn^{2+}-related $^4T_1 \rightarrow {}^6A_1$ transitions, which are responsible for the intense orange-yellow photoluminescence. Mn^{2+} doping significantly enhances the QE owing to efficient energy transfer from the ZnSe host to the Mn^{2+} luminescent centers, reducing non-radiative recombination pathways. Ag^{+} Substitution: With largest ionic radius among the dopants, Ag^{+} incorporation leads to pronounced lattice expansion and the formation of defect states within the ZnSe host material. These defects create additional donor-acceptor recombination pathways, contributing to the blue-shifted emission compared to that of undoped ZnSe. However, because of the competing non-radiative recombination processes, Ag^{+} doping results in a relatively lower QE than that of Mn^{2+} and Ni^{2+}-doped ZnSe QDs. The differences in lattice distortions, defect formations, and electronic state modifications caused by each dopant directly affect the emission characteristics and fluorescence efficiencies of ZnSe:X QDs. This tunability allows for tailored optoelectronic applications, including high-performance display technologies, bioimaging, and white-light LED applications.

As a result, in the absorption and emission spectra of ZnSe:X (X: Ni, Co, Mn, Ag), in addition to the lines and bands associated with the recombination of free excitons and excitons linked to the neutral donor and acceptor levels, there are broad bands associated with the 3d shell of X^{n+} ions (Scheme 3). The luminous center of X^{n+} in ZnSe is prominent at various wavelengths depending on the doping metal [54,55].

Thus, Ni, Co, Mn, and Ag doping into ZnSe improved the fluorescence efficiency of ZnSe QDs and altered their emission color under UV light. This will broaden the scope of the application of ZnSe nanoparticles after metal doping.

Table 2. Fluorescence quantum efficiency of ZnSe:5%Ni MPA QDs, ZnSe:5%Co MPA QDs, ZnSe:5%Mn MPA QDs, ZnSe:5%Ag MPA QDs.

Samples	Fluorescence quantum efficiency (%)
ZnSe:5%Ni MPA	34.56
ZnSe:5%Co MPA	28.79
ZnSe MPA	13.46
ZnSe:5%Mn MPA	49.52
ZnSe:5%Ag MPA	22.48

4. Conclusion

This study investigated the influence of Ni, Co, Mn, and Ag doping on the structural, optical, and photoluminescence properties of ZnSe quantum dots. X-ray diffraction confirmed that all doped ZnSe QDs retained the cubic zinc-blende crystal structure, with peak shifts due to lattice

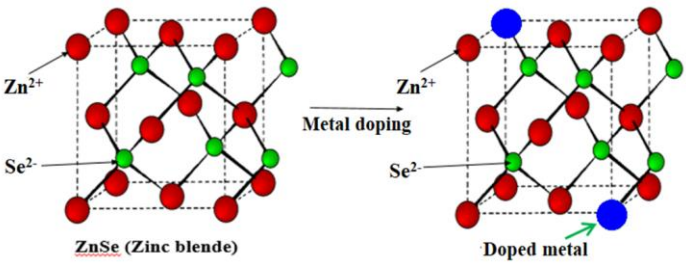

Scheme 2. X^{n+} ion-doping model of ZnSe MPA QDs.

strain from dopant incorporation. Ni^{2+} and Co^{2+} doping induced peak broadening and shifted toward higher angles, suggesting lattice contraction, while Mn^{2+} and Ag^{+} doping shifted the peaks toward lower angles, indicating expansion. Optical absorption studies showed that Ni^{2+} and Co^{2+} doping caused a blue shift in the absorption edge, increasing the effective bandgap energy owing to quantum confinement effects and lattice contraction. Mn^{2+} and Ag^{+} doping led to a redshift, which was attributed to the impurity levels and lattice expansion. Photoluminescence analysis showed that Mn^{2+} doping produced the most intense orange-yellow emission owing to the $^4T_1 \rightarrow {}^6A_1$ transition, with the highest fluorescence quantum efficiency (49.52%). Ni^{2+} and Co^{2+} doping introduced intermediate states, facilitating charge-carrier recombination and enhancing blue and yellow-green fluorescence, respectively. Ag^{+} doping exhibited moderate quantum efficiency owing to defect-related nonradiative recombination pathways, leading to a lower emission intensity. CIE color coordinate analysis validated the tunability of the emission wavelengths across the visible spectrum. Ni^{2+}-doped ZnSe QDs exhibited blue emission near (0.15, 0.09), Co^{2+}-doped showed greenish-yellow at (0.37, 0.49), Mn^{2+}-doped demonstrated strong orange-yellow at (0.52, 0.42), and Ag^{+}-doped exhibited, blue-shifted emission at (0.20, 0.15). These results confirm that selective doping allows precise control of the optical properties of ZnSe QDs, making them suitable for display applications, white-light LEDs, and bioimaging.

Declaration of Conflicting Interest

The authors have no competing interest to declare.

Data Availability Statement

This data is available upon request.

Acknowledgement

The authors acknowledge the Industrial University of Ho Chi Minh City, Vietnam for supporting this work (funding no. 23.1HH03).

CRediT Author Statement

Author Contributions: Thi Diem Bui (Conceptualization, Writing - Review & Editing, Supervision), Quang Liem Nguyen (Writing - Original Draft), Nguyen Van Cuong (Data Curation, Writing - Original Draft), Trong Tang Nguyen (Data Curation), Phuc Huu Dang (Writing - Review & Editing). All authors have read and agreed to the published version of the manuscript.

References

[1] Singh, S.B., Limaye, M. V., Date, S.K., Gokhale, S., Kulkarni, S.K. (2009). Iron substitution in CdSe nanoparticles: Magnetic and optical properties. *Physical Review B*, 80(23), 235421. DOI: 10.1103/PhysRevB.80.235421.

[2] Van, H.T., Vinh, N.D., Ca, N.X., Hien, N.T., Luyen, N.T., Do, P.V., Khien, N.V. (2020). Effects of ligand and chemical affinity of S and Se precursors on the shape, structure and optical properties of ternary CdS1−xSex alloy nanocrystals. *Materials Letters*, 264, 127387. DOI: 10.1016/j.matlet.2020.127387.

[3] Ca, N.X., Van, H.T., Do, P. V., Thanh, L.D., Tan, P.M., Truong, N.X., Oanh, V.T.K., Binh, N.T., Hien, N.T. (2020). Influence of precursor ratio and dopant concentration on the structure and optical properties of Cu-doped ZnCdSe-alloyed quantum dots. *RSC Advances*, 10(43), 25618–25628. DOI: 10.1039/D0RA04257A.

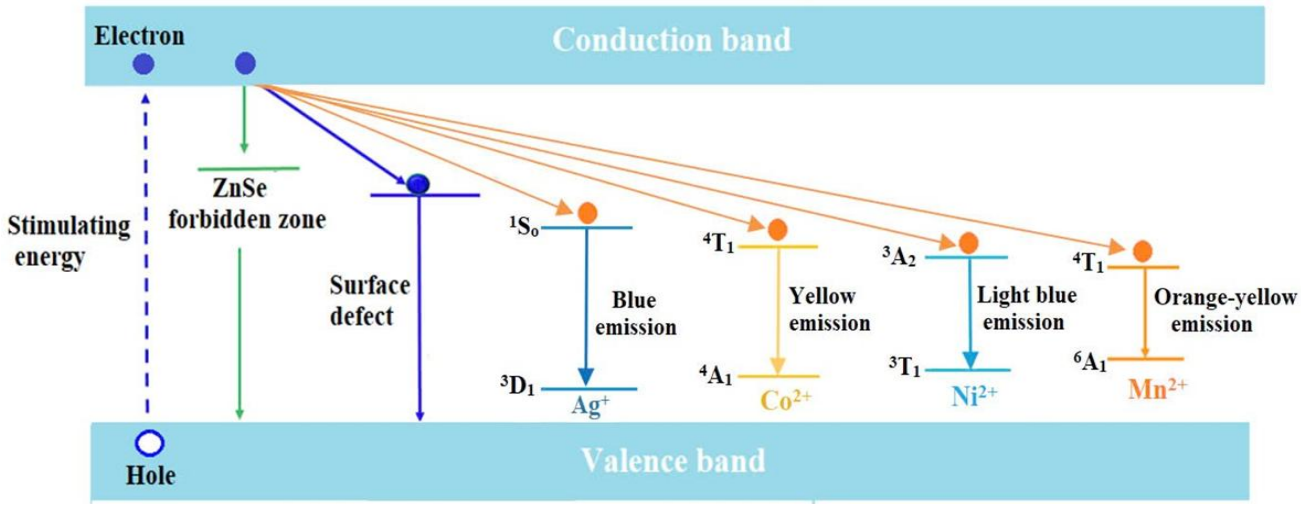

Scheme 3. Diagrammatic representation of emission transitions in ZnSe MPA QDs doped with metal.

[4] Das, S., Mandal, K.C. (2012). Optical downconversion in rare earth (Tb3+ and Yb3+) doped CdS nanocrystals. *Materials Letters*, 66(1), 46–49. DOI: 10.1016/j.matlet.2011.08.034.

[5] Memon, U.B., Chatterjee, U., Gandhi, M.N., Tiwari, S., Duttagupta, S.P. (2014). Synthesis of ZnSe Quantum Dots with Stoichiometric Ratio Difference and Study of its Optoelectronic Property. *Procedia Materials Science*, 5, 1027–1033. DOI: 10.1016/j.mspro.2014.07.393.

[6] Memon, U.B., Chatterjee, U., Gandhi, M.N., Tiwari, S., Duttagupta, S.P. (2014). Synthesis of ZnSe Quantum Dots with Stoichiometric Ratio Difference and Study of its Optoelectronic Property. *Procedia Materials Science*, 5, 1027–1033. DOI: 10.1016/j.mspro.2014.07.393.

[7] Baum, F., da Silva, M.F., Linden, G., Feijo, D., Rieder, E.S., Santos, M.J.L. (2019). Growth dynamics of zinc selenide quantum dots: the role of oleic acid concentration and synthesis temperature on driving optical properties. *Journal of Nanoparticle Research*, 21(2), 42. DOI: 10.1007/s11051-019-4485-6.

[8] Vempuluru, N.R., Kwon, H., Parnapalle, R., Urupalli, B., Munnelli, N., Lee, Y., Marappan, S., Mohan, S., Murikinati, M.K., Muthukonda Venkatakrishnan, S., Kim, K., Ahn, C.W., Yang, J.-M. (2024). ZnS/ZnSe heterojunction photocatalyst for augmented hydrogen production: Experimental and theoretical insights. *International Journal of Hydrogen Energy*, 51, 524–539. DOI: 10.1016/j.ijhydene.2023.08.249.

[9] Lin, S., Li, J., Pu, C., Lei, H., Zhu, M., Qin, H., Peng, X. (2020). Surface and intrinsic contributions to extinction properties of ZnSe quantum dots. *Nano Research*, 13(3), 824–831. DOI: 10.1007/s12274-020-2703-2.

[10] Zahra, T., Alanazi, M.M., Alahmari, S.D., Abdelmohsen, S.A.M., Abdullah, M., Aman, S., Al-Sehemi, A.G., Henaish, A.M.A., Ahmad, Z., Tahir Farid, H.M. (2024). Hydrothermally synthesized ZnSe@FeSe nanocomposite: A promising candidate for energy storage devices. *International Journal of Hydrogen Energy*, 59, 97–106. DOI: 10.1016/j.ijhydene.2024.01.293.

[11] El-assar, M., Taha, T.E., El-Samie, F.E.A., Fayed, H.A., Aly, M.H. (2023). ZnSe-based highly-sensitive SPR biosensor for detection of different cancer cells and urine glucose levels. *Optical and Quantum Electronics*, 55, 76. DOI: 10.1007/s11082-022-04326-y

[12] Hien, N.T., Tan, P.M., Van, H.T., Lien, V.T.K., Do, P.V., Loan, P.N., Kien, N.T., Luyen, N.T., Ca, N.X. (2020). Photoluminescence properties of Cu-doped CdTeSe alloyed quantum dots versus laser excitation power and temperature. *Journal of Luminescence*, 218, 116838. DOI: 10.1016/j.jlumin.2019.116838.

[13] Ca, N.X., Hien, N.T., Loan, P.N., Tan, P.M., Thuy, U.T.D., Phan, T.L., Nguyen, Q.B. (2019). Optical and Ferromagnetic Properties of Ni-Doped CdTeSe Quantum Dots. *Journal of Electronic Materials*, 48(4), 2593–2599. DOI: 10.1007/s11664-019-07017-9.

[14] Sheokand, S., Ahlawat, D.S., Singh, A. (2024). Nano structural and opto-magnetic investigation of Co–Ni co-doped ZnSe for spintronics. *Micro and Nanostructures*, 186, 207740. DOI: 10.1016/j.micrna.2023.207740.

[15] Muruganandam, S., Parivathini, K., Murugadoss, G. (2021). Effect of co-doped (Ni2+:Co2+) in CdS nanoparticles: investigation on structural and magnetic properties. *Applied Physics A*, 127(6), 400. DOI: 10.1007/s00339-021-04555-0.

[16] Thu Huong, T.T., Loan, N.T., Loc, D.X., Dieu Thuy, U.T., Stoilova, O., Liem, N.Q. (2021). Enhanced luminescence in electrospun polymer hybrids containing Mn-doped ZnSe/ZnS nanocrystals. *Optical Materials*, 113, 110858. DOI: 10.1016/j.optmat.2021.110858.

[17] Qiao, F., Kang, R., Liang, Q., Cai, Y., Bian, J., Hou, X. (2019). Tunability in the Optical and Electronic Properties of ZnSe Microspheres via Ag and Mn Doping. *ACS Omega*, 4(7), 12271–12277. DOI: 10.1021/acsomega.9b01539.

[18] Tavakkoli Yaraki, M., Tayebi, M., Ahmadieh, M., Tahriri, M., Vashaee, D., Tayebi, L. (2017). Synthesis and optical properties of cysteamine-capped ZnS quantum dots for aflatoxin quantification. *Journal of Alloys and Compounds*, 690, 749–758. DOI: 10.1016/j.jallcom.2016.08.158.

[19] Wang, C., Xu, S., Wang, Y., Wang, Z., Cui, Y. (2014). Aqueous synthesis of multilayer Mn:ZnSe/Cu:ZnS quantum dots with white light emission. *J. Mater. Chem. C*, 2(4), 660–666. DOI: 10.1039/C3TC31602E.

[20] Abd El-sadek, M.S., Nooralden, A.Y., Moorthy Babu, S., Palanisamy, P.K. (2011). Influence of different stabilizers on the optical and nonlinear optical properties of CdTe nanoparticles. *Optics Communications*, 284(12), 2900–2904. DOI: 10.1016/j.optcom.2011.01.071.

[21] Rabinovich, D. (2000). Advanced Inorganic Chemistry, 6th Edition (Cotton, F. A.; Wilkinson, G.; Murillo, C. A.; Bochmann, M.). *Journal of Chemical Education*, 77(3), 311. DOI: 10.1021/ed077p311.

[22] Jean-Louis Basdevant James Rich Michel Spiro (2004). *Fundamentals In Nuclear Physics*. Polytechnique.

[23] McCloskey, J.T., Newman, M.C., Clark, S.B. (1996). Predicting the relative toxicity of metal ions using ion characteristics: Microtox® bioluminescence assay. *Environmental Toxicology and Chemistry*, 15(10), 1730–1737. DOI: 10.1002/etc.5620151011.

[24] Rabinovich, D. (2000). Advanced Inorganic Chemistry, 6th Edition (Cotton, F. A.; Wilkinson, G.; Murillo, C. A.; Bochmann, M.). *Journal of Chemical Education*, 77(3), 311. DOI: 10.1021/ed077p311.

[25] Jean-Louis Basdevant, M.S.J.R. (2005). *Fundamentals In Nuclear Physics*. New York: Springer-Verlag.

[26] Blume, G., Cevc, G. (1993). Molecular mechanism of the lipid vesicle longevity in vivo. *Biochimica et Biophysica Acta (BBA) - Biomembranes*, 1146(2), 157–168. DOI: 10.1016/0005-2736(93)90351-Y.

[27] Geszke, M., Murias, M., Balan, L., Medjahdi, G., Korczynski, J., Moritz, M., Lulek, J., Schneider, R. (2011). Folic acid-conjugated core/shell ZnS:Mn/ZnS quantum dots as targeted probes for two photon fluorescence imaging of cancer cells. *Acta Biomaterialia*, 7(3), 1327–1338. DOI: 10.1016/j.actbio.2010.10.012.

[28] Zhang, B.-H., Wu, F.-Y., Wu, Y.-M., Zhan, X.-S. (2010). Fluorescent Method for the Determination of Sulfide Anion with ZnS:Mn Quantum Dots. *Journal of Fluorescence*, 20(1), 243–250. DOI: 10.1007/s10895-009-0545-0.

[29] Chandrakar, R.K., Baghel, R.N., Chandra, V.K., Chandra, B.P. (2015). Synthesis, characterization and photoluminescence studies of Mn doped ZnS nanoparticles. *Superlattices and Microstructures*, 86, 256–269. DOI: 10.1016/j.spmi.2015.07.043.

[30] Sundaresan, A., Bhargavi, R., Rangarajan, N., Siddesh, U., Rao, C.N.R. (2006). Ferromagnetism as a universal feature of nanoparticles of the otherwise nonmagnetic oxides. *Physical Review B*, 74(16), 161306. DOI: 10.1103/PhysRevB.74.161306.

[31] Arda, L. (2019). The effects of Tb doped ZnO nanorod: An EPR study. *Journal of Magnetism and Magnetic Materials*, 475, 493–501. DOI: 10.1016/j.jmmm.2018.11.121.

[32] Velumani, S., Narayandass, S.K., Mangalaraj, D. (1998). Structural characterization of hot wall deposited cadmium selenide thin films. *Semiconductor Science and Technology*, 13(9), 1016–1024. DOI: 10.1088/0268-1242/13/9/009.

[33] Paufler, P.P. (2006). Solid state chemistry: an introduction. 3rd Edition. By Lesley E. Smart and Elaine A. Moore. Pp. 407. Boca Raton: Taylor and Francis CRC Press, 2005. Price (softcover) USD 69.95. ISBN 0 748 77516 1. *Journal of Applied Crystallography*, 39(2), 288–288. DOI: 10.1107/S002188980600152X.

[34] Hamizi, N.A., Johan, M.R., Ghazali, N., Abdul Wahab, Y., Chowdhury, Z.Z., Akbarzadeh, O., Sagadevan, S., Badruddin, I.A., Yunus Khan, T.M., Kamangar, S. (2019). Lattice Strain Analysis of a Mn-Doped CdSe QD System Using Crystallography Techniques. *Processes*, 7(10), 639. DOI: 10.3390/pr7100639.

[35] Lange, H., Kelley, D.F. (2020). Spectroscopic Effects of Lattice Strain in InP/ZnSe and InP/ZnS Nanocrystals. *The Journal of Physical Chemistry C*, 124(41), 22839–22844. DOI: 10.1021/acs.jpcc.0c07145.

[36] Shen, H., Wang, H., Li, X., Niu, J.Z., Wang, H., Chen, X., Li, L.S. (2009). Phosphine-free synthesis of high quality ZnSe, ZnSe/ZnS, and Cu-, Mn-doped ZnSe nanocrystals. *Dalton Transactions*, (47), 10534. DOI: 10.1039/b917674h.

[37] Ca, N.X., Van, H.T., Do, P. V., Thanh, L.D., Tan, P.M., Truong, N.X., Oanh, V.T.K., Binh, N.T., Hien, N.T. (2020). Influence of precursor ratio and dopant concentration on the structure and optical properties of Cu-doped ZnCdSe-alloyed quantum dots. *RSC Advances*, 10(43), 25618–25628. DOI: 10.1039/D0RA04257A.

[38] Mondal, P., Sathiyamani, S., Das, S., Viswanatha, R. (2023). Electronic structure study of dual-doped II–VI semiconductor quantum dots towards single-source white light emission. *Nanoscale*, 15(37), 15288–15297. DOI: 10.1039/D3NR03542E.

[39] Lee, G.-J., Anandan, S., Masten, S.J., Wu, J.J. (2014). Sonochemical Synthesis of Hollow Copper Doped Zinc Sulfide Nanostructures: Optical and Catalytic Properties for Visible Light Assisted Photosplitting of Water. *Industrial & Engineering Chemistry Research*, 53(21), 8766–8772. DOI: 10.1021/ie500663n.

[40] Nguyen, T.P., Lam, Q.V., Vu, T.B. (2018). Effects of precursor molar ratio and annealing temperature on structure and photoluminescence characteristics of Mn-doped ZnS quantum dots. *Journal of Luminescence*, 196, 359–367. DOI: 10.1016/j.jlumin.2017.12.060.

[41] Bansal, N., Mohanta, G.C., Singh, K. (2017). Effect of Mn 2+ and Cu 2+ co-doping on structural and luminescent properties of ZnS nanoparticles. *Ceramics International*, 43(9), 7193–7201. DOI: 10.1016/j.ceramint.2017.03.007.

[42] Kuzmin, A., Dile, M., Laganovska, K., Zolotarjovs, A. (2022). Microwave-assisted synthesis and characterization of undoped and manganese doped zinc sulfide nanoparticles. *Materials Chemistry and Physics*, 290, 126583. DOI: 10.1016/j.matchemphys.2022.126583.

[43] Murugadoss, G. (2011). Synthesis, optical, structural and thermal characterization of Mn2+ doped ZnS nanoparticles using reverse micelle method. *Journal of Luminescence*, 131(10), 2216–2223. DOI: 10.1016/j.jlumin.2011.03.048.

[44] Tavakkoli Yaraki, M., Tayebi, M., Ahmadieh, M., Tahriri, M., Vashaee, D., Tayebi, L. (2017). Synthesis and optical properties of cysteamine-capped ZnS quantum dots for aflatoxin quantification. *Journal of Alloys and Compounds*, 690, 749–758. DOI: 10.1016/j.jallcom.2016.08.158.

[45] Pike, N.A., Pachter, R., Martinez, A.D., Cook, G. (2022). Computational analysis of the optical response of ZnSe with d-orbital defects. *Journal of Physics: Condensed Matter*, 34(20), 205402. DOI: 10.1088/1361-648X/ac594a.

[46] Pradhan, N., Das Adhikari, S., Nag, A., Sarma, D.D. (2017). Luminescence, Plasmonic, and Magnetic Properties of Doped Semiconductor Nanocrystals. *Angewandte Chemie International Edition*, 56(25), 7038–7054. DOI: 10.1002/anie.201611526.

[47] Mercey, G., Verdelet, T., Renou, J., Kliachyna, M., Baati, R., Nachon, F., Jean, L., Renard, P.-Y. (2012). Reactivators of Acetylcholinesterase Inhibited by Organophosphorus Nerve Agents. *Accounts of Chemical Research*, 45(5), 756–766. DOI: 10.1021/ar2002864.

[48] Yan, J., Estévez, M.C., Smith, J.E., Wang, K., He, X., Wang, L., Tan, W. (2007). Dye-doped nanoparticles for bioanalysis. *Nano Today*, 2(3), 44–50. DOI: 10.1016/S1748-0132(07)70086-5.

[49] Pechstedt, K., Whittle, T., Baumberg, J., Melvin, T. (2010). Photoluminescence of Colloidal CdSe/ZnS Quantum Dots: The Critical Effect of Water Molecules. *The Journal of Physical Chemistry C*, 114(28), 12069–12077. DOI: 10.1021/jp100415k.

[50] Grabolle, M., Spieles, M., Lesnyak, V., Gaponik, N., Eychmüller, A., Resch-Genger, U. (2009). Determination of the Fluorescence Quantum Yield of Quantum Dots: Suitable Procedures and Achievable Uncertainties. *Analytical Chemistry*, 81(15), 6285–6294. DOI: 10.1021/ac900308v.

[51] Pons, T., Lequeux, N., Mahler, B., Sasnouski, S., Fragola, A., Dubertret, B. (2009). Synthesis of Near-Infrared-Emitting, Water-Soluble CdTeSe/CdZnS Core/Shell Quantum Dots. *Chemistry of Materials*, 21(8), 1418–1424. DOI: 10.1021/cm8027127.

[52] Kubin, R.F., Fletcher, A.N. (1982). Fluorescence quantum yields of some rhodamine dyes. *Journal of Luminescence*, 27(4), 455–462. DOI: 10.1016/0022-2313(82)90045-X.

[53] Demasa, J.N., Crosby, G.A. (1971). The Measurement of Photoluminescence Quantum Yields. A Review. *The Journal of Physical Chemistry*, 75, 8, 15 April, 991-1024. DOI: 10.1021/j100678a001.

[54] Zeng, R., Zhang, T., Dai, G., Zou, B. (2011). Highly Emissive, Color-Tunable, Phosphine-Free Mn:ZnSe/ZnS Core/Shell and Mn:ZnSeS Shell-Alloyed Doped Nanocrystals. *The Journal of Physical Chemistry C*, 115(7), 3005–3010. DOI: 10.1021/jp111288h.

[55] Kubin, R.F., Fletcher, A.N. (1982). Fluorescence quantum yields of some rhodamine dyes. *Journal of Luminescence*, 27(4), 455–462. DOI: 10.1016/0022-2313(82)90045-X..